

Robustness and accuracy of cell division in *Escherichia coli* in diverse cell shapes

Jaan Männik^{a,b}, Fabai Wu^a, Felix J. H. Hol^a, Paola Bisicchia^c, David J. Sherratt^c, Juan E. Keymer^a, and Cees Dekker^{a,1}

^aDepartment of Bionanoscience, Kavli Institute of Nanoscience, Delft University of Technology, Lorentzweg 1, 2628 CJ Delft, The Netherlands; ^bDepartment of Physics and Astronomy, University of Tennessee, 1408 Circle Drive, Knoxville, TN 37996; and ^cDepartment of Biochemistry, University of Oxford, South Parks Road, Oxford OX1 3QU, United Kingdom

Edited by Kiyoshi Mizuuchi, National Institute of Diabetes and Digestive and Kidney Diseases, Bethesda, MD, and approved March 15, 2012 (received for review December 20, 2011)

Cell division in typical rod-shaped bacteria such as *Escherichia coli* shows a remarkable plasticity in being able to adapt to a variety of irregular cell shapes. Here, we investigate the roles of the Min system and the nucleoid-occlusion factor SlmA in supporting this adaptation. We study “squeezed” *E. coli* in narrow nanofabricated channels where these bacteria exhibit highly irregular shapes and large volumes. Despite the severely anomalous morphologies we find that most of these bacteria maintain their ability to divide into two equally sized daughters with an accuracy comparable to that of normal rod-shaped cells (about 4%). Deletion of either *slmA* or *minC* shows that the molecular systems associated with these genes are largely dispensable for accurate cell division in these irregular cell shapes. Using fluorescence time-lapse microscopy, we determine that the functionality of the Min system is affected by the cell shape, whereas the localization of a nucleoid relative to the cell division proteins (the divisome) remains unperturbed in a broad spectrum of morphologies, consistent with nucleoid occlusion. The observed positioning of the nucleoid relative to the divisome appears not to be affected by the nucleoid-occlusion factor SlmA. The current study underscores the importance of nucleoid occlusion in positioning the divisome and shows that it is robust against shape irregularities.

cytokinesis | FtsZ | lab-on-a-chip | microfluidics

In cell division, which is one of the most critical cellular processes in bacteria, the accurate and robust spatial organization of proteins is essential (1, 2). Divisome proteins—i.e., the proteins that mediate bacterial cytokinesis (3–5)—must be positioned such that each daughter cell inherits a fully functional genome. Experimentally, it has been found that the divisome localizes very accurately near the center of many prokaryotic cells such as *Escherichia coli* (6–8). Rod-shaped *E. coli* have been shown to divide into two almost equally sized daughter cells that have average length differences as small as 1.3% (7).

Two molecular mechanisms—the Min system and nucleoid occlusion—have been identified as playing roles in localizing the divisome in prokaryotic cells (3–5). In *E. coli*, the Min system consists of three proteins MinC, MinD, and MinE. In a rod-shaped cell, these proteins oscillate periodically between the two poles of a bacterium (9), producing a time-averaged concentration profile that has local maxima at the cell poles. Of these three proteins, MinC has been shown to antagonize divisome formation (10) by blocking the polymerization of the FtsZ protein, a key component of the divisome that recruits other members of the complex (5). It has been established that a high average density of MinC provides an inhibitory signal that prevents localization of the divisome at the cell poles where cell division would otherwise lead to the disadvantageous formation of nucleoid-free minicells. The dynamic behavior of the Min system has been explained by a molecular model that takes into account diffusion of MinCDE in the cytosol, cooperative binding of MinD to the membrane, and its subsequent unbinding by MinE (11, 12). Recently, the finding that diffusion plays a limited role in oscillatory waves of MinD

in a reconstituted *in vitro* system has led to an alternative model based on initiation and dissociation complexes (13).

Complementary to the Min system, nucleoid occlusion has been shown to be important in ensuring accurate cell division (7, 14). This mechanism is based on the phenomenological observations that the nucleoid (i.e., the bacterial chromosome) inhibits the formation of a divisome in its immediate neighborhood (15, 16). How the nucleoid exactly interacts with the divisome remains a matter of debate. The DNA-binding protein SlmA (17) has been proposed to mediate nucleoid occlusion either by binding to FtsZ protofilaments (18) or by breaking down the protofilaments in the cytosol (19). Interestingly, it has been found that the binding of SlmA to bacterial DNA is sequence specific (18, 19). The absence of SlmA binding sites near the *terC* region and enhanced activity of SlmA in depolymerizing FtsZ filaments in the DNA-bound form suggest a possible mechanism for its function in positioning the bacterial FtsZ ring. In addition to SlmA, MukB (14) and DnaA proteins (17, 20) have also been shown to play a role in this phenomenon, yet the underlying molecular mechanisms have not been elucidated. It has also been proposed that nucleoid occlusion is mediated by a transection mechanism, where DNA is tethered to the membrane through transcribed RNAs and their amphiphilic products that inhibit the assembly of the bacterial divisome in the vicinity of nucleoid-occupied space (16, 21).

Perhaps even more remarkable than the accuracy of division in rod-shaped cells is the robustness of cell division that occurs in aberrant forms of bacteria. We have recently shown that in channels of submicron depth, *E. coli* transform from rods to a variety of irregular cell shapes whose lateral dimensions can exceed 5 μm (22). Despite their complex shapes, these cells, surprisingly, are still able to divide and partition their chromosomes. Here, we address to what extent the Min system and the nucleoid-occlusion mechanism can adapt and function in these irregular cell shapes. For this purpose, we determine the accuracy of cell divisions in these squeezed *E. coli*, and compare the findings from this phenotype to the findings from normal rod-shaped cells as well as to findings from mutant cells where the Min system or the nucleoid-occlusion factor SlmA is deleted. We also use quantitative fluorescence time-lapse imaging of the nucleoid, the FtsZ, and the MinD proteins to understand the role of these molecular systems in complicated cell shapes. The great variety of morphologies exhibited by squeezed *E. coli* makes these cells a particularly suitable model for this study. The large size and flat shape of these cells furthermore facilitates microscopy, allowing for data analy-

Author contributions: J.M., J.E.K., and C.D. designed research; J.M. and F.W. performed research; J.M., F.J.H.H., P.B., and D.J.S. contributed new reagents/analytic tools; J.M. analyzed data; and J.M. and C.D. wrote the paper.

The authors declare no conflict of interest.

This article is a PNAS Direct Submission.

¹To whom correspondence should be addressed. E-mail: c.dekker@tudelft.nl.

This article contains supporting information online at www.pnas.org/lookup/suppl/doi:10.1073/pnas.1120854109/-DCSupplemental.

sis with a higher accuracy than that for aberrant morphologies studied in the past and even for normal rod-shaped cells.

Results

To study both regular rod-shaped and squeezed *E. coli* cells, we use microfabricated silicon chips. We image bacteria in two types of structures etched into these chips: microchambers and shallow channels (Fig. 1A and B). The rod-shaped phenotype (Fig. 1C) populates microchambers whose depth (ca. 1.8 μm) exceeds the diameter of the bacteria (ca. 0.8 μm). Transformation to a squeezed phenotype occurs in shallow channels with a depth of about 0.25 μm where bacteria are squeezed by the walls of the channel. (Note that the bacteria are able to deform the ceiling of these channels. The height of the channels in the presence of bacteria is higher than 0.25 μm .) The transformation to the squeezed phenotype consists of two phases (23). Upon entering the channels, the cells undergo a mechanical deformation and widen along their short axis by 30–40%. This initial deformation is followed by a much slower continuous broadening, which becomes significant after about one cell cycle, when a progeny cell may already reach twice its original width. This slow broadening, which could be a result of remodeling of the cell wall under mechanical stress, can after multiple cell divisions lead to very wide cells with a variety of aberrant non-rod-shaped morphologies (Fig. 1D and SI Appendix, Fig. S1). Not all cells in the channels transform to very wide shapes (e.g., cells on the left of Fig. 1D), but those that are at the front of the expanding population in the channel primarily do. In this frontal population, the broadest cells reach diameters of about 5 μm (22), whereas cells farther behind show a relatively minor broadening (diameters ca. 1.0 μm). Such variation in cell widths allows a study of cell division across the entire range of very large squeezed cells to the normal rod-shaped phenotype.

Despite their aberrant shapes, the squeezed cells are still able to divide with generation times close to those of the rod-shaped cells in microchambers (22). Only exceptionally broad cells, whose apparent diameters exceed approximately 5 μm , show initiation but then subsequent stalling of cell wall constrictions. Although the aberrant squeezed cells below approximately 5- μm diameter are capable of dividing, one would perhaps expect,

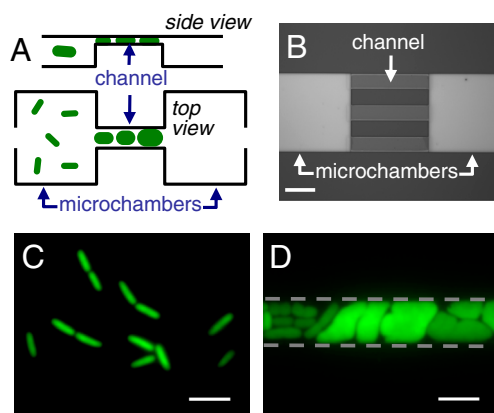


Fig. 1. (A) Schematics of the experiment. The top shows a cross-sectional view and the bottom a top view of a microfluidic chip and bacteria (green). The microfluidic chip consists of two distinct structures: deeper microchambers (typical depth 1.8 μm) and shallow channels (typical depth 0.25 μm). In deeper microchambers, the bacteria are not mechanically confined and they show the normal rod-shaped morphology, whereas in the shallow channels bacteria are squeezed by the channel walls and transform to broad and irregular shapes (Middle). (B) Microscope image of a microfluidic chip showing the shallow channels and deeper microchambers. (Scale bar: 20 μm .) (C) Fluorescent image of GFP-labeled *E. coli* BW25113 in the microchambers. (D) Fluorescent image of the same strain in shallow channels of 0.25- μm depth. Scale bars in C and D correspond to 5 μm .

based on observations of filamentous (15) and multibranched *E. coli* (24), that these cells would partition much less symmetrically into daughter cells than their wild-type counterparts. To examine the degree of symmetry, we quantify how accurately the volume of the mother cell partitions into two daughters for both the normal and squeezed phenotypes. We define the division ratio as the ratio of the volume of one daughter cell (V_{daughter}) to the total volume of the two daughter cells right after division (V_{mother}). We assume that the total fluorescence intensity of the cytosolic GFP scales with the cell volume, and we take the ratio of these intensities in two daughter cells equal to the ratio of cell volumes (SI Appendix, Materials and Methods).

The resulting histograms for the division ratios (Fig. 2A and B) show a pronounced central peak at value 0.50, which corresponds to the equal partitioning of the mother cell into two daughters. The data for cells with a squeezed phenotype (Fig. 2B) show, besides the central peak, longer tails with discernible small peaks at division ratios of about 0.25 and 0.75. These cells, despite their irregular shapes, are able to give rise to daughter cells with 1:1 but also with 1:3 volumetric ratios. Next we analyze how accurately the cells that divide about their volumetric center partition their cell volumes. For this analysis, we define the central peak in the histograms as all the data points that fall in the range of division ratios from 0.375 to 0.625. These boundaries represent midpoints between the locations of the central peaks with division ratio 0.5 and the two side peaks with division ratios 0.25 and 0.75. We find that 99% of all divisions in regular and 90% of divisions in squeezed cells count as central divisions. Comparing the widths of the central peaks shows that the two have essentially equal widths in normal ($\sigma = 0.037$) and squeezed phenotypes ($\sigma = 0.037$). We note that the experimental error in determining the division accuracy is 0.005, which is negligibly smaller than the width of central peak (SI Appendix, Materials and Methods). Thus, surprisingly, for these cells that divide around their volumetric

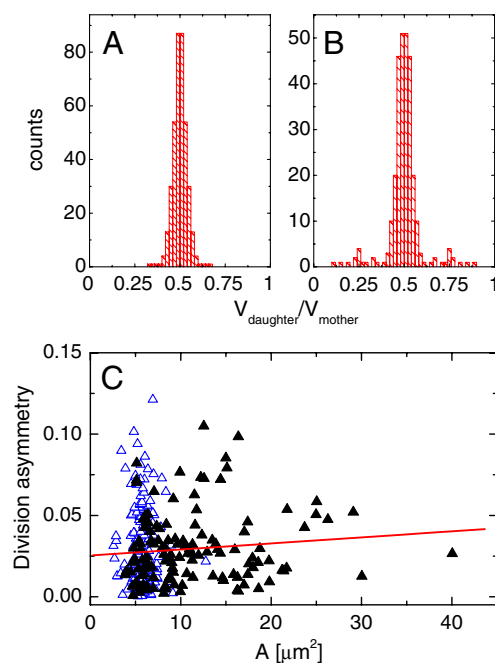


Fig. 2. Accuracy of cell division in rod-shaped and squeezed cells. Histograms of daughter-to-mother cell-volume ratios ($V_{\text{daughter}}/V_{\text{mother}}$) for (A) normal and (B) squeezed *E. coli* BW25113 cells. Both daughter cells are counted in the histograms. (C) Division asymmetry vs. the measured area of the mother cells for centrally occurring divisions. Blue open triangles are data for rod-shaped cells, and black filled squares are for squeezed cells. The line is a linear fit for the data from squeezed cells ($y = 0.00037x + 0.025$; $R = 0.11$, $p = 0.22$).

center, the accuracy of the division in *E. coli* is not compromised in the irregularly shaped squeezed phenotype compared to their normal rod-shaped counterparts.

The data in the histograms of Fig. 2 *A* and *B* are collected for all cell sizes. To quantify the possible effect of cell size on cell division, we plot the division asymmetry for centrally occurring divisions, defined as $|0.5 - V_{\text{daughter}}/V_{\text{mother}}|$, versus the apparent area of the mother cell (Fig. 2*C*). Note that the apparent area is determined from the cell contours and not from the fluorescence intensities (*SI Appendix, Materials and Methods*). From linear regression, we find coefficients between cell area and division asymmetry $R = -0.013$ for normal and $R = 0.11$ for squeezed cells, with the probabilities that there is no correlation between the cell area and division asymmetry being $p = 0.85$ and $p = 0.22$, respectively. When taking into account all the cell divisions (*SI Appendix, Fig. S2*), a stronger correlation between accuracy and cell size can be seen ($R = 0.62$; $p < 10^{-5}$). This higher correlation coefficient results from more divisions taking place with 1:3 and higher volumetric ratios in larger cells. Thus, although the cell division shows a tendency to become more asymmetric, the accuracy of central divisions is only marginally affected by cell size even when the cell volume becomes five times larger than in typical rod-shaped cells (for estimation of cell volumes, see *SI Appendix, Fig. S3*).

It is also of interest to compare the asymmetry of partitioning of cytosolic material with the asymmetry of partitioning of chromosomes. Note that the chromosomal mass need not partition symmetrically in these squeezed *E. coli* cells because of their multiploidy. We infer multiploidy of these cells from observing multiple *terC* loci in larger squeezed cells in *E. coli* (*SI Appendix, Fig. S4*). Plotting the division accuracy of cytosol vs. the division accuracy of chromosomal mass for the same cell (*SI Appendix, Fig. S5*), we find from a linear regression a correlation coefficient of 0.90. The cytosolic and chromosomal parts of the cell thus divide in a highly correlated manner. This finding suggests that chromosomal distribution is the underlying organizational pattern that drives the localization of the divisome in large and irregularly shaped squeezed cells.

Next we investigate the effect that deletion of either the Min system or the nucleoid-occlusion mediating factor SlmA has on the accuracy of cell division. For this study we use the *minC* null mutant strain JW1165, which shows a typical minicelling phenotype, and the *slmA* null mutant JW5641-1 (25) (*SI Appendix,*

Table S1). We find that the *SlmA*-deficient strain shows essentially the same behavior in both phenotypes as its parental strain does (*SI Appendix, Fig. S6* and *Tables S2* and *S3*). The only observed difference for the *SlmA*-deficient strain is a more significant trend ($R = 0.21$, $p = 0.02$) of cell division asymmetry on the cell area (*SI Appendix, Table S4*).

The rod-shaped phenotype in the *minC* deletion strain shows a smaller number of central partitions than its parental strain. Now 73% of all cells divide with an approximately 1:1 volume ratio whereas the parental strain showed 99% of such events (*SI Appendix, Fig. S7* and *Table S2*). From the noncentrally occurring divisions, 49% occur with approximately 1:3 volumetric ratio whereas the remainder, mostly minicell leading divisions, count for 51%. The accuracy of central divisions ($\sigma = 0.041$) turns out to be lower at a statistically significant level compared to that of the parental strain without these deletions (*SI Appendix, Table S3*). In the irregularly shaped squeezed cells of the *MinC*⁻ strain, the number of central divisions decreases further, but the majority of cells (54%) are still able to divide by their volumetric center. Notably, however, the accuracy of central divisions does not change at a significant level when compared to nonsqueezed cells of the same phenotype (*SI Appendix, Table S3*). Thus, the deletion of either the Min system or *slmA* does not lead to an increased loss of accuracy in the central divisions in squeezed cells in comparison to the rod-shaped phenotype of the same mutant.

To further understand the role of the Min system in positioning the divisome in irregularly shaped squeezed cells, we study the localization patterns of MinD-GFP over time and compare this to regular cells. In regular cells, as previously reported (9), we observe periodic oscillations of the MinD concentration resulting in a high time-averaged accumulation of MinD at the cell poles (Fig. 3 *A* and *B*, and *Movie S1*). Although squeezed cells with slight irregularities in their morphology show the same pattern as regular rod-shaped cells, this is not always the case in more complicated cell shapes. Fig. 3 *C–F* shows two examples of cell shapes wherein accumulation of MinD at the cell extremities is not apparent and where the positions of corresponding maxima do not form a regular pattern in space. The oscillations in these cases give rise to a larger number of less pronounced maxima (4–6) per cell in the time-averaged distributions (Fig. 3 *C* and *E*). Inspection of time-lapse images (*Movies S2* and *S3*, and Fig. 3, *Lower*) shows that the localization of MinD is not only

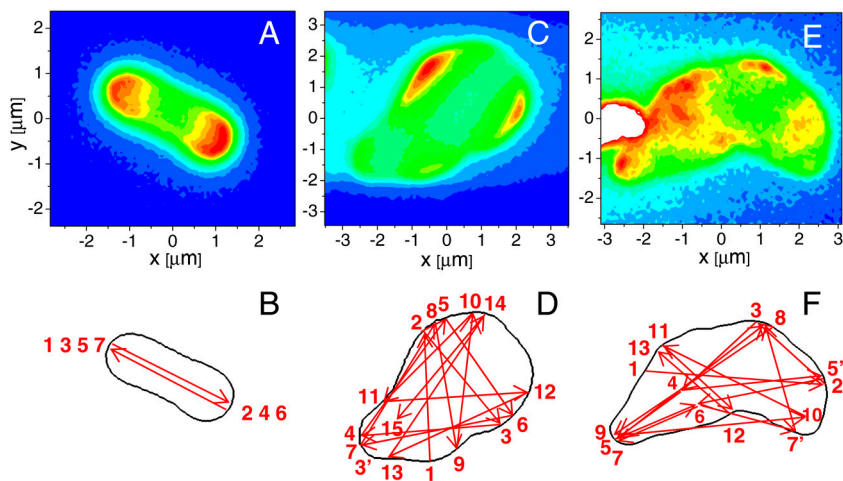


Fig. 3. MinD oscillations in rod-shaped and squeezed *E. coli* cells. The top row presents time-averaged spatial distributions of MinD-GFP in (*A*) rod-shaped, and (*C* and *E*) squeezed cells. The distributions are averaged over a total of 350 s, while sampling images every 10 s. Distributions are presented as heat maps for visualization (red color corresponds to high and blue to low MinD concentration). The white area in *E* corresponds to a different cell with a higher average level of MinD-GFP expression. *A* and *E* correspond to *E. coli* TG1 with plasmid pMW1255 and *C* to *E. coli* MC1000 with pFX4. (*B*, *D*, and *F*) Movements of MinD maxima as observed from time-lapse movies (*Movies S1–S3*) for the cells shown in the upper row. Arrows connect two consecutive maxima in time. Maxima are labeled by their order of appearance. If two maxima become visible at the same time, then one of the maxima is labeled by an extra prime index.

limited to these apparent maxima but also involves other positions, which are visited less frequently and therefore do not appear as distinct maxima in the time-averaged distributions (SI Appendix, Fig. S8). Although most of the time, a single MinD maximum relocates from one position to another, sometimes a maximum can split into two new ones (marked by prime indexes in Fig. 3, Lower). As a result of these more chaotic patterns, the time-averaged MinD distribution tends to be more spatially uniform for these squeezed cells than it is for rod-shaped cells (SI Appendix, Fig. S9). These results indicate that the Min system is unable to provide a well-defined pattern for cell division in some cell shapes that differ from the regular morphology.

To investigate the role of nucleoid occlusion in localizing the divisome, we image *E. coli* strain AND102 where the divisome and nucleoid are labeled by FtsZ-GFP (26) and HupA-RFP (HU-RFP; RFP, red fluorescent protein) proteins, respectively (SI Appendix, Table S1). HupA and DAPI labels have been shown to produce essentially identical images of the nucleoid (27), but with HupA-RFP, unlike with DAPI staining, it is possible to carry out time-lapse imaging because the cells remain viable during imaging. Two-color imaging of normal *E. coli* cells in microchambers (Fig. 4 A–D) shows the typical positioning of the FtsZ ring between two separated nucleoids. We observe a clear anticorrelation between the nucleoid and the FtsZ ring (Fig. 4D). According to the nucleoid-occlusion mechanism, the nucleoids should

separate first and FtsZ assembly will occur subsequently in the preformed gap between nucleoids. From time-lapse imaging of cells, as shown in Fig. 4 A–C (Movie S4), we indeed observe that a gap between nucleoids develops first. Consistent with the nucleoid-occlusion mechanism, the new FtsZ rings subsequently accumulate into these gaps. The observed gaps in the chromosomal distribution do not necessarily mean that chromosomes have fully replicated and segregated in these cells. Although such behavior has been suggested from studies of fixed cells (8, 28), this timing, to our knowledge, has not been reported directly in live cells before.

The chromosomal distributions in broader squeezed cells show a much more complex organization (Fig. 4E and Movie S5). Distinct features in the distribution of chromosomal density in wider cells (widths > 1.5 μm) are centrally localized voids (as shown by vertical arrows in Fig. 4). Despite the more complex distribution of chromosomal mass, FtsZ and the nucleoid still exhibit a strong spatial anticorrelation in these aberrant squeezed cells. Such anticorrelated localization becomes particularly striking in some broad *E. coli* where arced FtsZ structures can assemble into a curved gap between the chromosomal mass on both sides (e.g., in Fig. 4 E–G). Here, it appears that the asymmetric distribution of the chromosomal mass guides the positioning of the FtsZ arc. Arced FtsZ structures and incomplete rings have been observed in some mutant *E. coli* earlier (29) but here we observe these structures in nonmutant cells which have acquired large sizes as a result of mechanical stress.

We quantify the spatial anticorrelation between FtsZ and nucleoid by a Pearson correlation coefficient R_{nucl} between the line profiles of FtsZ and the nucleoid intensity distributions. These correlation coefficients are measured across the FtsZ arcs as indicated by the bars in Fig. 4 D and H (SI Appendix, Materials and Methods). The Pearson coefficient shows a clear negative correlation between the FtsZ and nucleoid profiles for all analyzed cases (Fig. 5 A and B), both for normal and squeezed cells. Interestingly, the average values and standard deviations of the R -value distributions are essentially the same for the normal cells ($R_{\text{nucl}} = -0.75 \pm 0.18$) and squeezed cells ($R_{\text{nucl}} = -0.78 \pm 0.14$). The indistinguishable distribution of the correlation coefficients in both cell types is a strong indicator that the nucleoid-occlusion mechanism is not perturbed by the changes in the cell shape.

To estimate the spatial scale over which the nucleoid and the divisome interact, we measure the widths of the FtsZ peaks and the dips in the nucleoid distribution from the line profiles such as shown in Fig. 4 D and H. From Gaussian fits to the peaks and dips, we determine the full-width at half-maximum for both types of structures (Fig. 5 C and D). FtsZ-intensity peaks have an average width of $W_{\text{FtsZ}} = 0.34 \pm 0.09 \mu\text{m}$ for normal cells and $W_{\text{FtsZ}} = 0.39 \pm 0.12 \mu\text{m}$ for squeezed cells. These widths are roughly 40% smaller than the average width of gaps in the nucleoid distributions, which are $W_{\text{nucleoid}} = 0.57 \pm 0.23 \mu\text{m}$ and $W_{\text{nucleoid}} = 0.65 \pm 0.23 \mu\text{m}$ for normal and squeezed cells, respectively. Note that all these numbers exceed the width of the point spread function (ca. 0.25 μm) of our imaging system. Comparison of W_{FtsZ} and W_{nucleoid} in normal and squeezed cells thus shows that their values are essentially the same in both phenotypes, which further supports the conclusion drawn from the correlation analysis that the nucleoid-occlusion mechanism is independent of cell morphology.

In analyzing the spatial distribution of the nucleoid and FtsZ, we have thus far considered data from all cells independently on how far the cell division has progressed in these cells, requiring only that the cell had visible FtsZ structures. Restricting the analysis to only those cells in which distinguishable FtsZ arcs or rings have just appeared (within a 5-min interval, whereas total cell generation time is approximately 75 min), we find for normal cells $W_{\text{FtsZ}} = 0.50 \pm 0.09 \mu\text{m}$ and $W_{\text{nucleoid}} = 0.51 \pm$

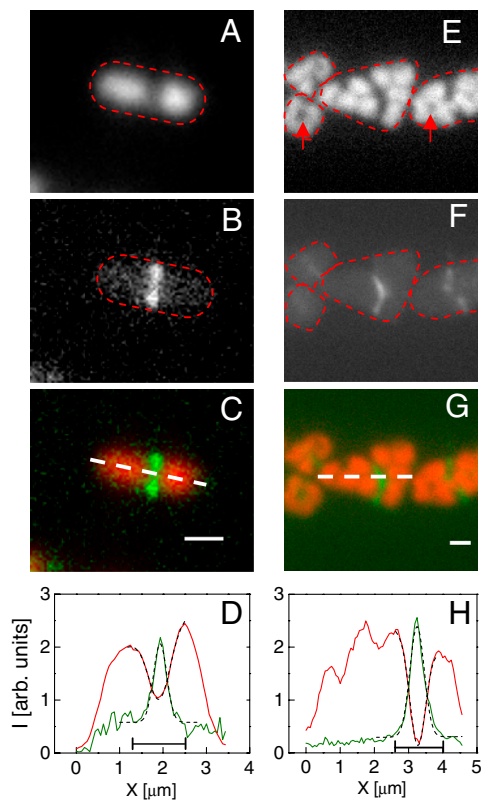


Fig. 4. Localization of nucleoid and FtsZ in rod-shaped (Left) and squeezed cells (Right). (A and E) HupA-RFP-labeled nucleoid, (B and F) FtsZ-GFP, and (C and G) composite overlay images. Dashed red lines show approximate contours of the bacteria. Note that the image of the normal cell is zoomed out twice compared to squeezed cells. Arrows in E point to central voids in the chromosome distribution. D and H are line profiles of the nucleoid (red) and FtsZ (green) densities. The line profiles are taken along the dashed lines which are indicated in the composite images. Dashed black lines correspond to Gaussian fits of the FtsZ peaks and the gaps in the chromosome distribution, respectively. The horizontal bars indicate the distance over which the Pearson correlation coefficient between the two curves is calculated. (Scale bar: 1 μm.)

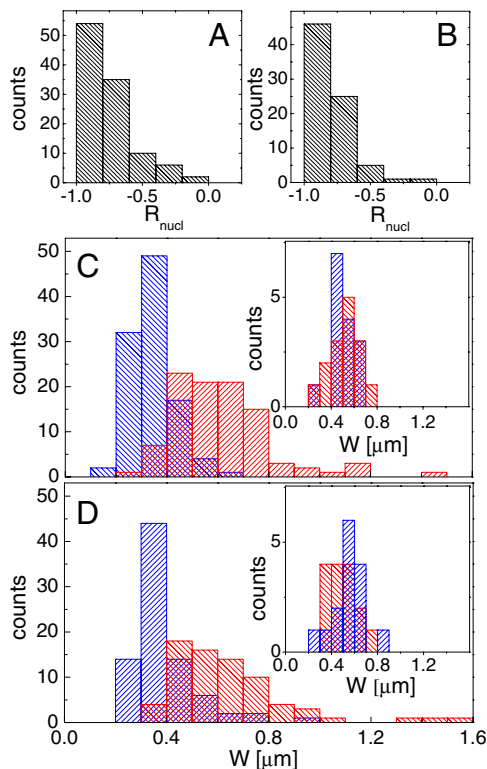


Fig. 5. Comparison of the nucleoid-occlusion mechanism in normal and squeezed cells. Pearson correlation coefficient (R_{nucl}) for (A) normal and (B) squeezed cells. The correlation coefficient is calculated over a distance of $1.2 \mu\text{m}$ around the intensity maximum of FtsZ (compare bar in Fig. 4 D and H). C and D display the width (W) of FtsZ peaks (blue) and the width of the gaps in nucleoid distribution (red) as determined by Gaussian fitting (black dashed lines in Fig. 4 D and H). The widths correspond to the full-width at half-maximum values of the fitted Gaussian profiles. (C) Distribution of widths for normal and (D) for squeezed *E. coli*. Data are acquired from 110 normal and 83 squeezed cells in various stages of their cell cycle. Inset in both panels shows the same distributions ($N = 15$ in both cases) for cells within 5 min of the first appearance of visible structures of FtsZ.

$0.12 \mu\text{m}$ (Fig. 5C, Inset), and for squeezed cells $W_{\text{FtsZ}} = 0.50 \pm 0.11 \mu\text{m}$ and $W_{\text{nucleoid}} = 0.54 \pm 0.14 \mu\text{m}$ (Fig. 5D, Inset). These values show that the widths of FtsZ bands and gaps in nucleoid distribution are of comparable size at the early phase of cell division when the FtsZ arcs start to form. As the cell cycle progresses, the gaps in the chromosomal distribution widen, while at the same time the FtsZ peaks become narrower. The initial formation of dips in the chromosomal distribution, and a subsequent tight filling of these regions with FtsZ, thus provide an indication that the nucleoid acts as a fine-scale template for the positioning of the bacterial divisome.

Finally, we investigate how the positioning of FtsZ relative to the nucleoid is affected by deletion of either the *minC* or the nucleoid-occlusion factor-encoding gene *slmA*. For that purpose, we study strains PB191 (*minC* deletion) and PB192 (*slmA* deletion), which express FtsZ-GFP and HupA-RFP (SI Appendix, Table S1). Carrying out the correlation analysis as described above, we find that *slmA* null mutants in both normal and squeezed phenotypes show indistinguishable R_{nucl} -value distributions (SI Appendix, Fig. S10) compared to the strain without such deletions (SI Appendix, Tables S5 and S6). Thus, the nucleoid-occlusion factor SlmA surprisingly does not affect the anticorrelated placement of the divisome relative to the nucleoid.

For the *minC*-deletion strain, a more complicated situation emerges due to divisions leading to minicells (SI Appendix, Fig. S11). Leaving out these divisions, the resulting distributions in both normal rod-shaped and irregular squeezed morphologies

are indistinguishable from the distribution in the strain where the Min system is intact (SI Appendix, Tables S5 and S6). On the other hand, those FtsZ rings that lead to minicells in the *minC*-deletion strain have a very limited correlation relative to the nucleoid distribution. The corresponding R_{nucl} -value distributions are broad and centered at $R_{\text{nucl}} \approx 0$ for both the squeezed and rod-shaped phenotypes (SI Appendix, Fig. S11). The lack of anticorrelation in these cases shows that nucleoid occlusion plays no role in the placement of the divisome in the nucleoid-free regions near the poles, as can be expected. With the exception of these minicell divisions, the anticorrelated location of the nucleoids relative to the FtsZ rings appears to be unaffected by deletions of either *minC* or *slmA*. Moreover, the correlations between the two systems are also not affected by changes in cell morphology that take place during the transition from the regular rod-shapes to the irregular squeezed cells.

Discussion

Our data show the remarkable ability of wild-type *E. coli* to carry out cell division in very large and irregular morphologies. The majority of observed divisions occurred around the volumetric center of the mother cell. Although the frequency of central divisions decreased with the increasing cell size, the accuracy of this type of division remained essentially unaffected by the shape and size of the cell. To understand what mechanisms are responsible for the accurate and robust positioning of the divisome in these cells, we studied strains that lacked either a functional Min system or the nucleoid-occlusion factor SlmA. The accuracy of central divisions remained unchanged for both *slmA* and *minC* deleted cells when it was compared to the regular phenotype of the same mutant cells, indicating that both molecular systems have a limited role in the placement of divisome around their volumetric center in these irregularly shaped cells. On the other hand, we found that the Min system is important in the placement of the divisome in normal rod-shaped cells. Consistent with the earlier report (30), we observed a loss of accuracy in the placement of the divisome in *MinC*⁻ strain compared to wild-type strain when cells were not squeezed. These observations for the squeezed and the normal cells together imply that although effective in normal morphologies, the Min system loses some of its function in more complicated cell shapes.

To further understand the Min system in complex cell shapes, we investigated the spatial and temporal distributions of MinD in squeezed *E. coli*. In several irregular morphologies such as almost-spheroid (31) or Y-shaped cells (24), it was previously concluded that the Min system can still provide a reliable positional signal. In contrast, we find that in many aberrant squeezed cells MinD local maxima oscillate in space without a well-defined stationary pattern. Reminiscent of the chaotic billiard problem in classical mechanics, the trajectories of the MinD maximum (arrows on Fig. 3 A–C) did not converge to a periodic orbit in these bacteria. The time-averaged distribution of MinD, however, was not completely homogeneous, but showed accumulation of MinD maxima at certain preferred locations. Surprisingly, these maxima did not always coincide with what can be considered the polar regions in these aberrant cells. This finding further agrees with our previous assessment that, although the Min system can in certain geometries provide a reliable signal for the placement of divisome, it fails in others and cannot be considered a robust mechanism to locate the cell division site.

In contrast to the behavior displayed by the Min system, we find the same strong spatial anticorrelation between FtsZ and nucleoid distributions in very aberrant morphologies as in normal cell shapes in the wild-type strain. Moreover, in the beginning of cell division and independently of morphology, the peaks in FtsZ and gaps in nucleoid density have essentially identical widths. From these observations, nucleoid occlusion appears to provide a generally applicable mechanism for localization of divisome in a

variety of aberrant morphologies of *E. coli*. In terms of the recently proposed model of nucleoid occlusion based on the SlmA protein and its specific binding to loci near *oriC* region (18, 19), this result is not obvious. In multiploid cells, where chromosomes including *oriC* and *terC* regions (SI Appendix, Fig. S4) are not organized in a well-defined regular pattern, one would expect the effectiveness of SlmA to localize the divisome and the correlations between nucleoid and FtsZ to be diminished.

How can the nucleoid-occlusion mechanism achieve the partitioning of cells into two daughters with nearly equal volumes or volumes that scale as the ratio of two integers? Our data are highly suggestive that the underlying mechanism relies on the discrete nature of chromosomes. In polyploid cells, the two daughters each inherit an integer number of fully replicated nucleoids, provided the chromosomes are not cut during cell division. The inspection of many time-lapse movies with concurrent FtsZ-GFP and nucleoid labels does not support the latter scenario—we find nucleoids that are well cleared from the cell division site before the completion of cytokinesis in these aberrant cells. Because we find that the amount of chromosomal mass and the cytosolic volume are well correlated in squeezed cells ($R = 0.90$; SI Appendix, Fig. S5), and because the nucleoids partition as discrete quantities, it follows that the cytosolic volumes of the two daughter cells scale as ratios of integer numbers. For smaller mother cells that accommodate a smaller number of nucleoids, the highest likelihood for dividing is a 1 : 1 volume ratio for the two daughter cells. For very large cells with a large number of nucleoids, an unequal numbers of nucleoids in the two daughter cells becomes a possible outcome as well, explaining the tendency of these cells to divide their cytosol with 1 : 3 and higher volumetric ratios.

Despite its important role in cell division, the interactions through which the nucleoid exerts inhibitory signals to the divisome are not well understood. SlmA proteins clearly play an active role in mediating these interactions (17–19). We observe that the cell division accuracy decreases in SlmA mutant cells

with increasing cell size more significantly than in wild-type cells. At the same time, however, we notice that the correlation between placement of the nucleoid and FtsZ is not affected by deletion of *slmA* both in regular rod-shaped and squeezed phenotypes. The latter observation rules out that SlmA acts as the only or even the major contributor to nucleoid occlusion. This conclusion is also corroborated with the earlier findings that SlmA is not an essential protein and is conditionally lethal with the deletion of the Min system only for *E. coli* growing in LB but not in minimal M9 medium (17).

In summary, our work shows, remarkably, that *E. coli* bacteria retain a high accuracy in partitioning their cell volumes, even when their cell shape is strongly perturbed. Although the Min system is important in positioning of the bacterial divisome in rod-shaped cells, we find its role limited in irregular cell morphologies. The robust accuracy in cell division likely stems from the discreteness of the bacterial nucleoid and indicates the importance of nucleoid occlusion in the positioning of the bacterial divisome. A detailed understanding of molecular mechanisms involved in nucleoid occlusion, which are not limited to the known factor SlmA, deserves yet a comprehensive study.

Materials and Methods

Details of bacterial growth conditions, microchip design, fluorescence microscopy setup, and image analysis are given in the SI Appendix, Materials and Methods. The list of all strains and plasmids used in this study, including their sources, is given in the SI Appendix, Table S1.

ACKNOWLEDGMENTS. The authors thank S. Donkers and I. Westerlaken for technical assistance; A. Dajkovic (Institute Curie, Paris), M. Loose (Technische Universität Dresden), R. Reyes-Lamothe (University of Oxford), Y.L. Shih (Academia Sinica), and S. Aleexeva and C. L. Woldringh (University of Amsterdam) for generous gifts of strains and plasmids; and R. Reyes-Lamothe and C. L. Woldringh for valuable discussions. This work has been supported in part by research grants from European Science Foundation/European Collaborative Research Synbio (780) and the European Research Council NanoforBio (247072).

- Shapiro L, McAdams HH, Losick R (2009) Why and how bacteria localize proteins. *Science* 326:1225–1228.
- Moseley JB, Nurse P (2010) Cell division intersects with cell geometry. *Cell* 142:189–193.
- Adams DW, Errington J (2009) Bacterial cell division: Assembly, maintenance and disassembly of the Z ring. *Nat Rev Microbiol* 7:642–653.
- Lutkenhaus J (2007) Assembly dynamics of the bacterial MinCDE system and spatial regulation of the Z ring. *Annu Rev Biochem* 76:539–562.
- Margolin W (2005) FtsZ and the division of prokaryotic cells and organelles. *Nat Rev Mol Cell Biol* 6:862–871.
- Trueba FJ (1982) On the precision and accuracy achieved by Escherichia coli-cells at fission about their middle. *Arch Microbiol* 131:55–59.
- Yu XC, Margolin W (1999) FtsZ ring clusters in min and partition mutants: Role of both the Min system and the nucleoid in regulating FtsZ ring localization. *Mol Microbiol* 32:315–326.
- Den Blaauwen T, Buddelmeijer N, Aarsman MEG, Hameete CM, Nanninga N (1999) Timing of FtsZ assembly in Escherichia coli. *J Bacteriol* 181:5167–5175.
- Raskin DM, de Boer PAJ (1999) Rapid pole-to-pole oscillation of a protein required for directing division to the middle of Escherichia coli. *Proc Natl Acad Sci USA* 96:4971–4976.
- Shen B, Lutkenhaus J (2010) Examination of the interaction between FtsZ and MinCN in E-coli suggests how MinC disrupts Z rings. *Mol Microbiol* 75:1285–1298.
- Huang KC, Meir Y, Wingreen NS (2003) Dynamic structures in Escherichia coli: Spontaneous formation of MinE rings and MinD polar zones. *Proc Natl Acad Sci USA* 100:12724–12728.
- Kerr RA, Levine H, Sejnowski TJ, Rappel WJ (2006) Division accuracy in a stochastic model of Min oscillations in Escherichia coli. *Proc Natl Acad Sci USA* 103:347–352.
- Ivanov V, Mizuuchi K (2010) Multiple modes of interconverting dynamic pattern formation by bacterial cell division proteins. *Proc Natl Acad Sci USA* 107:8071–8078.
- Sun Q, Yu XC, Margolin W (1998) Assembly of the FtsZ ring at the central division site in the absence of the chromosome. *Mol Microbiol* 29:491–503.
- Woldringh CL, et al. (1990) Role of the nucleoid in the toporegulation of division. *Res Microbiol* 141:39–49.
- Zaritsky A, Woldringh CL (2003) Localizing cell division in spherical Escherichia coli by nucleoid occlusion. *FEMS Microbiol Lett* 226:209–214.
- Bernhardt TG, de Boer PAJ (2005) SlmA, a nucleoid-associated, FtsZ binding protein required for blocking septal ring assembly over chromosomes in *E. coli*. *Mol Cell* 18:555–564.
- Tonthat NK, et al. (2011) Molecular mechanism by which the nucleoid occlusion factor, SlmA, keeps cytokinesis in check. *EMBO J* 30:154–164.
- Cho HB, McManus HR, Dove SL, Bernhardt TG (2011) Nucleoid occlusion factor SlmA is a DNA-activated FtsZ polymerization antagonist. *Proc Natl Acad Sci USA* 108:3773–3778.
- Moriya S, Rashid RA, Rodrigues CDA, Harry EJ (2010) Influence of the nucleoid and the early stages of DNA replication on positioning the division site in Bacillus subtilis. *Mol Microbiol* 76:634–647.
- Sun Q, Margolin W (2004) Effects of perturbing nucleoid structure on nucleoid occlusion-mediated toporegulation of FtsZ ring assembly. *J Bacteriol* 186:3951–3959.
- Männik J, Driessen R, Galajda P, Keymer JE, Dekker C (2009) Bacterial growth and motility in sub-micron constrictions. *Proc Natl Acad Sci USA* 106:14861–14866.
- Männik J, Sekhvatvi F, Keymer JE, Dekker C (2010) Bacteria in submicron channels and microvalves. *Proc of MicroTAS 2010, Groningen, The Netherlands* pp 1346–1348.
- Varma A, Huang KC, Young KD (2008) The Min system as a general cell geometry detection mechanism: Branch lengths in Y-shaped Escherichia coli cells affect Min oscillation patterns and division dynamics. *J Bacteriol* 190:2106–2117.
- Baba T, et al. (2006) Construction of Escherichia coli K-12 in-frame, single-gene knockout mutants: The Keio collection. *Mol Syst Biol* 2:1–11.
- Dajkovic A, Mukherjee A, Lutkenhaus J (2008) Investigation of regulation of FtsZ assembly by SlnA and development of a model for FtsZ polymerization. *J Bacteriol* 190:2513–2526.
- Wery M, Woldringh CL, Rouviere-Yaniv J (2001) HU-GFP and DAPI co-localize on the Escherichia coli nucleoid. *Biochimie* 83:193–200.
- Inoue I, Ino R, Nishimura A (2009) New model for assembly dynamics of bacterial tubulin in relation to the stages of DNA replication. *Genes Cells* 14:435–444.
- Addinall SG, Lutkenhaus J (1996) FtsZ-spirals and -arcs determine the shape of the invaginating septa in some mutants of Escherichia coli. *Mol Microbiol* 22:231–237.
- Guberman JM, Fay A, Dworkin J, Wingreen NS, Gitai Z (2008) PSICIC: Noise and asymmetry in bacterial division revealed by computational image analysis at sub-pixel resolution. *PLoS Comput Biol* 4:e1000233.
- Corbin BD, Yu XC, Margolin W (2002) Exploring intracellular space: Function of the Min system in round-shaped Escherichia coli. *EMBO J* 21:1998–2008.

